THERMAL MODELLING AND CHARACTERISATION OF SEMICONDUCTOR BOLOMETERS

R V Sudiwala, M J Griffin, and A L Woodcraft

Department of Physics and Astronomy, University of Wales, Cardiff, 5 The Parade, Cardiff CF 24 3YB, UK

International Journal of Infrared and Millimeter Waves, 23(4):545-573, 2002

Abstract: A revised version of the Griffin & Holland ideal semiconductor bolometer model is presented and its use in determining bolometer properties and parameters from experimental load curve measurements is discussed. We show that degeneracy between some bolometer parameters can only be broken by model fitting a family of load curves over a range of bath temperatures, and that measurements with the bolometer blanked (zero absorbed radiant power) are essential for unambiguous determination of the main parameters. The influence of measurement errors on parameter recovery is analysed using synthetic noisy data sets.

Keywords: Cryogenic detectors, Bolometers, NTD.

1 Introduction

Low temperature semiconductor bolometers are widely used in ground, balloon, and satellite based millimetre and sub-millimetre wave astronomy [e.g., Refs. 1, 2, 3]. Silicon nitride micromesh bolometers using neutron transmutation doped (NTD) germanium thermistors operating at 100-300 mK are arguably the current mature state-of-the-art technology [e.g., Refs. 4, 5, 6, 7].

The physical principles of cryogenic semiconductor bolometers have been developed by Jones [8], Low [9], and Mather [10, 11]. Based on Mather's non-equilibrium theory, Chanin & Torre [12] and Griffin & Holland [13] developed parameterised ideal thermal bolometer models to investigate optimisation under different levels of radiant background power loading. This work was extended by Grannan et al. [14] to include electrical non-linearities. Whilst these works provide a good theoretical framework for bolometer design, the issue of detailed characterisation and performance verification of actual devices needs further discussion. To this end, we present a modified form of the Griffin & Holland model and discuss its use in characterising actual devices. We use synthetic voltage-current data sets to illustrate important aspects of design and performance verification, and demonstrate the applicability of an ideal thermal model to real bolometers. We also discuss non-thermal electrical effects that might account for the departures of real devices from ideal thermal behaviour. Application of the model to the characterisation of a prototype bolometer for the 143-GHz band of the Planck HFI instrument is described by Woodcraft et al. [7].

2 Bolometer thermal model

A bolometric detector is shown schematically in Figure 1. A thermistor of resistance R and at temperature T is coupled to a heat sink at a bath temperature T_0 through a thermal link of length L and static thermal conductance G_S. A bias current I flows through the thermistor, generating a voltage $V = IR$ across it. The bias current is usually generated by load resistance R_L in series with a voltage source V_a. The voltage V is usually measured through a low noise voltage amplifier. The total power dissipated in the bolometer is $W = P + Q$ where Q is the absorbed radiant power and $P = VI$ is the electrical power. The bolometer has heat capacity $C(T)$ (we assume that the thermal link has zero heat capacity).

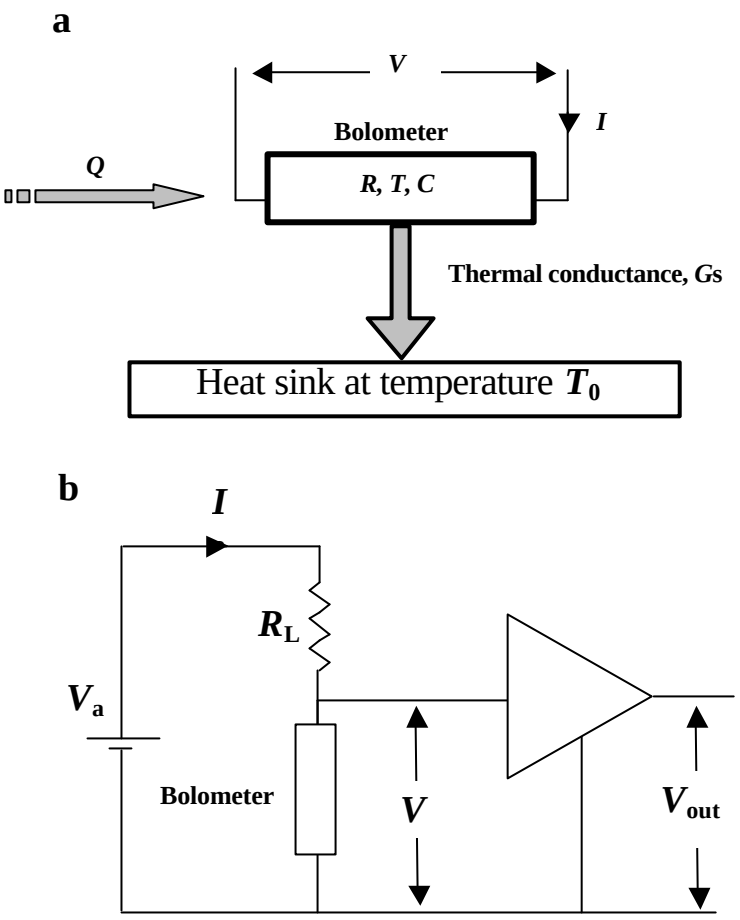

Figure 1: Schematic diagrams of (a) a bolometric detector and (b) the electrical bias and measuring circuit.

The steady state energy balance equation for the bolometer is

$$W = G_S\left(T - T_0\right). \tag{1}$$

The Griffin & Holland model was based on the non-equilibrium bolometer theory of Mather [10] but assumed that the variation of the thermal conductance with temperature can be expressed as a power law, $G_S(T,T_0) = G_{S0}(T/T_0)^b$ where G_{S0} is the thermal conductance at temperature $T = T_0$. Here, in keeping with Mather's theory, we make the physically more realistic assumption, also noted by Murray et al. [15] and Grannan et al. [14], that it is the temperature variation of the thermal conductivity, k, of the thermal link that is appropriately expressed as a power law:

$$k(T) = k_0\left(\frac{T}{T_0}\right)^b, \tag{2}$$

where $k_0 = k(T_0)$. In other words we take the variation of thermal conductivity with temperature across the thermal link into account. Now,

$$W = \frac{\displaystyle\int_{T_0}^{T} k(t)\,\mathrm{d}t}{\displaystyle\int_0^L \frac{1}{A(x)}\,\mathrm{d}x}, \tag{3}$$

where $A(x)$ is the cross-sectional area of thermal link at position x. For simplicity, but without loss of generality, we take the cross section to be constant, $A(x) = A$. Integration of equation (3) then yields

$$W = \frac{A}{L}\frac{k_0 T_0}{(b+1)}\left(f^{b+1} - 1\right), \tag{4}$$

where $f = T/T_0$. From equations (1) and (4), we have

$$G_S(f) = \frac{A}{L}\frac{k_0}{(b+1)}\left(\frac{f^{b+1}-1}{f-1}\right) = \frac{G_{S0}}{(b+1)}\left(\frac{f^{b+1}-1}{f-1}\right), \tag{5}$$

where $G_{S0} = k_0(A/L)$ (which can be deduced by taking the limit $T \to T_0$ in equation (5) above). From equations (1) and (5) we obtain

$$P(f) = \frac{G_{S0}T_0}{(b+1)}\left(f^{b+1} - 1\right) - Q\,. \tag{6}$$

Equation (6) enables us to model the voltage-current (load curve) characteristics of a bolometer if we know the temperature variation of the thermistor resistance, $R(T)$.

A variety of doped semiconductors [14, 16] have been used as low temperature thermistor materials. The dominant conduction mechanism in these materials is variable range hopping between localised sites [17, 18, 19], and in general the resistance of the device varies with both applied voltage and temperature [14, 20]

$$R(T,V) = R^* \exp\left[\left(\frac{T_g}{T}\right)^n - \frac{eEL}{k_B T}\right], \tag{7}$$

where T_g is a material parameter, R^* depends on both material and device geometry, L is related to the average hopping distance and is in general temperature dependent [7] and E is the electric field across the device. In the absence of electrical non-linearities, and other effects such as electron-phonon decoupling [20], the thermistor resistance depends only on temperature:

$$R(T) = R^* \exp\left[\left(\frac{T_g}{T}\right)^n\right]. \tag{8}$$

Within the context of the ideal thermal bolometer model discussed here, we assume that the thermistor resistance varies only with temperature as described by equation (8).

The voltage-current characteristic (load curve) of an ideal thermal bolometer can be generated by incrementing T from T_0 to some value T_{max} in equations (6) and (8). For given values of b, G_{S0}, Q, R^*, T_g, and n, the electrical power P and resistance $R(T)$ can be determined. Then

$$V = [PR(T)]^{1/2}\,, \tag{9a}$$

and

$$I = [P/R(T)]^{1/2}. \tag{9b}$$

Other important quantities for specifying bolometer performance are as given below. The temperature coefficient of resistance of the bolometer, α, is given by

$$\alpha = \frac{1}{R}\frac{dR}{dT} = -\frac{nT_g^n}{T^{n+1}}\,. \tag{10}$$

The dynamic impedance, Z, is given by

$$Z = \frac{\mathrm{d}V}{\mathrm{d}I} = R\left[\frac{G_\mathrm{d} + aP}{G_\mathrm{d} - aP}\right], \tag{11}$$

where $G_\mathrm{d} = \mathrm{d}W/\mathrm{d}T$ is the dynamic thermal conductance at temperature T:

$$G_\mathrm{d}(T) = \left(\frac{A}{L}\right)k_0 f^b = G_{\mathrm{d}0} f^b, \tag{12}$$

and $G_{\mathrm{d}0} = G_\mathrm{d}(T_0) = (A/L)k_0$. We note that $G_{\mathrm{d}0} = G_{\mathrm{S}0}$ - i.e. the static and dynamic thermal conductances are the same at the bath temperature. The DC responsivity, S, is [8]

$$S = \frac{\mathrm{d}V}{\mathrm{d}Q} = \left[\frac{Z - R}{2V}\right]\left[\frac{R_\mathrm{L}}{Z + R_\mathrm{L}}\right], \tag{13a}$$

or equivalently,

$$S = \frac{aV}{G_\mathrm{e}}\left[\frac{R_\mathrm{L}}{R + R_\mathrm{L}}\right], \tag{13b}$$

where G_e, the effective thermal conductance, differs from G_d due to the effect of electro-thermal feedback [10]:

$$G_\mathrm{e} = G_\mathrm{d} - aP\left[\frac{R_\mathrm{L} - R}{R_\mathrm{L} + R}\right]. \tag{14}$$

Finally, the responsivity of the ideal bolometer varies with the angular frequency of modulation of the incident radiation, w, as:

$$S(w) = S(0)\left[1 + w^2 t_\mathrm{e}^2\right]^{-1/2}, \tag{15}$$

where the effective thermal time constant, τ_e, is given by

$$t_e = \frac{C}{G_\mathrm{e}}. \tag{16}$$

In the Appendix, these equations are used to express the responsivity in terms of the parameters b, n, T_g, R^*, $G_{\mathrm{S}0}$, and Q. The Appendix also examines the various contributions to the bolometer *NEP* and likewise relates these to the above parameters, and, for completeness, gives the modified forms of the equations used by Griffin & Holland [12] for bolometer optimisation, taking into account equation (2).

3 Bolometer characterisation

As discussed above, for a given a set of values for the parameters (b, n, T_g, R^*, G_{S0}, and Q) it is a simple matter to model a load curve at a bath temperature T_0 using equations (6), (8) and (9). Similarly, the responsivity and *NEP* as a function of bias current can also be also be modelled using equations (13), (14), (A10), (A11) and (A15). For the purpose of illustration, we consider a bolometer with the parameter summarised in Table I:

b	1.3
n	½
T_g	15 K
R^*	100 Ω
G_{S0}	120 pW K^{-1} at T_0 = 100 mK
Q	0 (blanked - i.e. no radiant loading) or 0.5 pW (non-blanked).

Table I: Parameter set used for model bolometer

For bolometers that use neutron-transmutation-doped germanium:gallium (NTD-Ge) thermistor elements in which the dominant conduction mechanism is variable range hopping, the value of n = ½ has been found to produce good fits to the R-T variation of over the range of temperatures of interest here and over several orders of magnitude in resistance [16,20]. Ideally, b = 1 for a metallic thermal link, or 3 for a crystalline dielectric link [21]; real bolometers may consist of a number of components with differing properties and so can exhibit values of b between these limits.

A typical set of measurements needed to characterise the performance of both the bolometer and its associated optical components comprises:

(i) blanked load curves, in which sets of voltage-current characteristics of the bolometer are measured for a variety of bath temperatures, T_0, ensuring that there is no power loading on the bolometer by external radiation;
(ii) non-blanked load curves, for which the bolometer views a controlled amount of external radiation (these are again recorded at various bath temperatures);
(iii) speed of response measurements, in which the frequency response of the bolometer to a modulated radiant source is recorded over a range of electrical bias voltages and for a variety of bath temperatures;
(iv) bolometer noise measurements on the bolometer, both blanked and non-blanked.

The goal of bolometer characterisation is to determine experimentally the parameter set of the bolometer.

4 Model fitting of a single load curve

To understand the importance of each of these data sets, it is worth considering how much can be learned just from a single load curve measurement. The measured load curve can be expressed as R vs. P. From equations (6) and (8), and using n = ½,

$$\ln\left[-R\frac{\mathrm{d}P}{\mathrm{d}R}\right] = -(2b+3)\ln\left[\ln\left[\frac{R}{R^*}\right]\right] + \ln\left[\frac{2G_{S0}T_g{}^{b+1}}{T_0{}^{b}}\right]. \qquad (17)$$

We presume to know only T_0. Equation (17) is linear in $\ln[\ln(R/R^*)]$, with slope $m = -(2b + 3)$ and intercept $c = \ln[2G_{so}T_g{}^{\beta+1}/T_0{}^{\beta}]$, only for the correct value of R^*. Thus, a graph of χ^2 vs. R^* from a linear least squares fit enables us to determine both R^* and b. This is illustrated in Figure 2 for both blanked and non-blanked synthetic load curves at T_0 = 100 mK using the standard parameter set listed above. We have determined the derivative numerically from the modelled data by differentiating an interpolation function of the R vs. P curve, just as we would for a measured load curve. The optimum recovered value for R^* is obtained by finding the minimum of the interpolated χ^2 vs. R^* curve. From Figure 2a we find an optimum value of $R^* = 100\ \Omega$ for both of the synthetic load curves as expected. Using this optimum value of R^* in equation (17) and applying a linear least squares fit, the best fit values of the slope and intercept can be found. Figure 2b shows that both synthetic load curves yield identical values of $m = 5.6$ and $c = 14.7$. From m, we determine $b = 1.3$ as expected. For the blanked load curve, in the limit $P \rightarrow 0$, the thermistor temperature $T \rightarrow T_0$ (equation 1) and $R(T, P \rightarrow 0) = R(T_0)$ which can be measured from the R-P curve. Thus, T_g can be deduced from equation (8) and hence G_{S0} from the value of the intercept c. From our synthetic blanked load curve, $R(T, P \rightarrow 0) \approx 2.08 \times 10^7\ \Omega$, giving values of T_g = 15 K and G_{S0} = 119.9 pW K^{-1} as expected. It is not possible to determine T_g and G_{S0} from a non-blanked load curve in this fashion because the thermistor temperature $T > T_0$ at $P = 0$. For the particular non-blanked load curve used here with Q = 0.5 pW, we find $R(T, P \rightarrow 0) \approx 1.6 \times 10^7\ \Omega$.

In principle, therefore, all of the bolometer parameters can determined from a single blanked load curve, and R^* and b can be determined even if it is not known that the load curve was blanked. In practice equation (17) is difficult to apply because it requires extremely low-noise data. The double logarithm means that the method is insensitive to R^*. Synthetic data show that the load curves need to be measured to better than 0.05% accuracy and with a sampling interval small enough to enable the numerical derivative to be calculated reliably. This is illustrated for our example bolometer with synthetic blanked load curves calculated at T_0 = 100 mK with noise added at the 0.01% and 0.1% levels for each voltage and current datum. Figures 3a and 3b show a typical χ^2 vs. R^* curve, and the least squares fit to equation (17) using the optimum value of R^* derived from it, respectively, for the case of 0.01% noise level. The average from a set of five such synthetic load curves yielded $R^* = 95 \pm 8.2\ \Omega$, $m = 5.63 \pm 0.04$, and c = 14.8 ± 0.16. From these values we find $b = 1.31 \pm 0.02$, $T_g = 15.1 \pm 0.2$ K, and $G_{S0} = 120.6 \pm 0.8$ pW K^{-1}, which agree very well with the original parameter set. Figure 3c shows a typical χ^2 vs. R^* curve for a 0.1% noise level case giving an optimum value of R^* =

46.9 Ω. The least square fit using this value is shown in Figure 3d from which we find b = 1.5, T_g = 16.9 K, and G_{S0} = 127.5 pW K^{-1}. The relatively large differences between these best fit values and the actual parameters mean that these numbers would be unsuitable for predicting the bolometer behaviour at other base temperatures. We have been unable to find a smoothing algorithm or other method to make the numerical determination of the derivative more accurate.

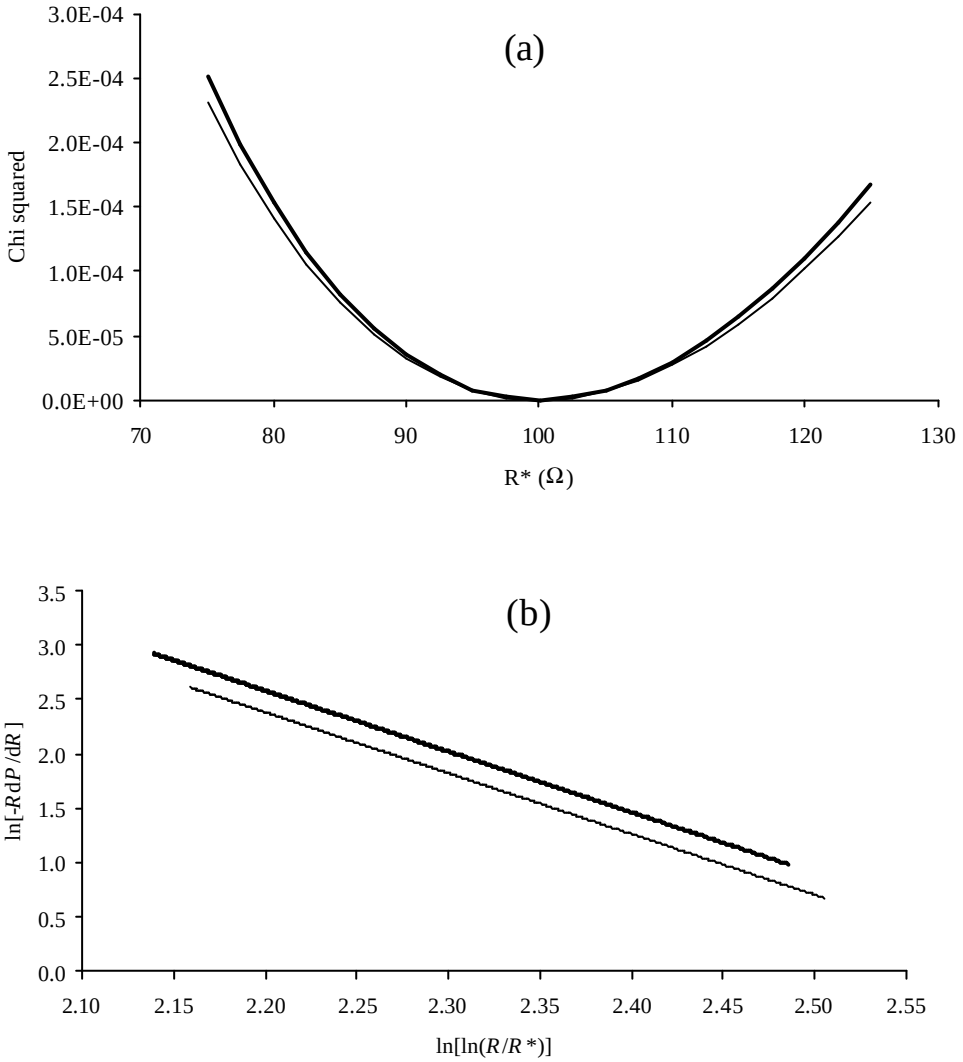

Figure 2: (a) χ^2 vs. R^* for fits to equation (17) for data from synthetic load curves generated using the standard parameter set at T_0 = 100 mK. Lighter curve: Q = 0 (blanked); heavier curve: Q = 0.5 pW (non-blanked). Both curves show a minimum in χ^2 at a "best" value of R^* = 100 Ω as expected. (b) The load curve data plotted

according to equation (17) using the "best" value of $R^* = 100\ \Omega$ as found above. Lighter line: Q = 0; heavier line (which has been displaced by 0.2 units in the vertical scale for clarity) Q = 0.5 pW. Both curves have the same slope and intercept.

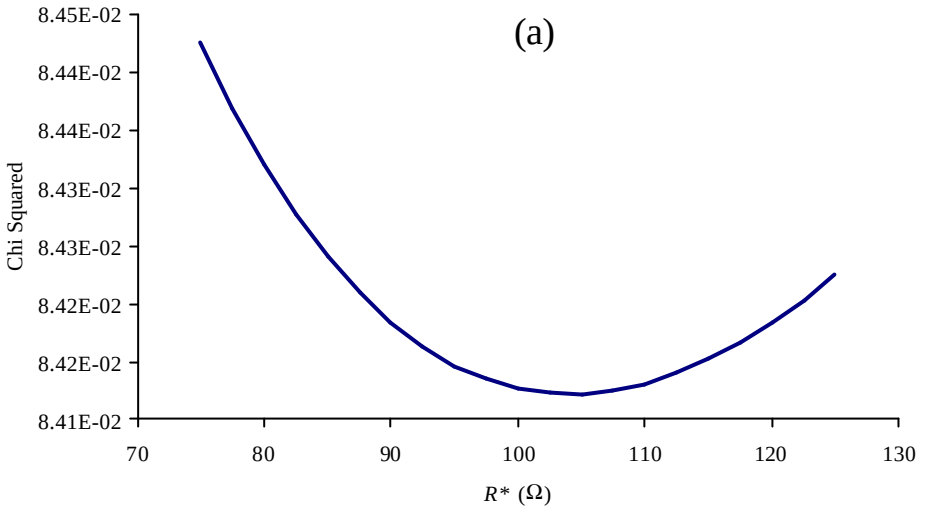

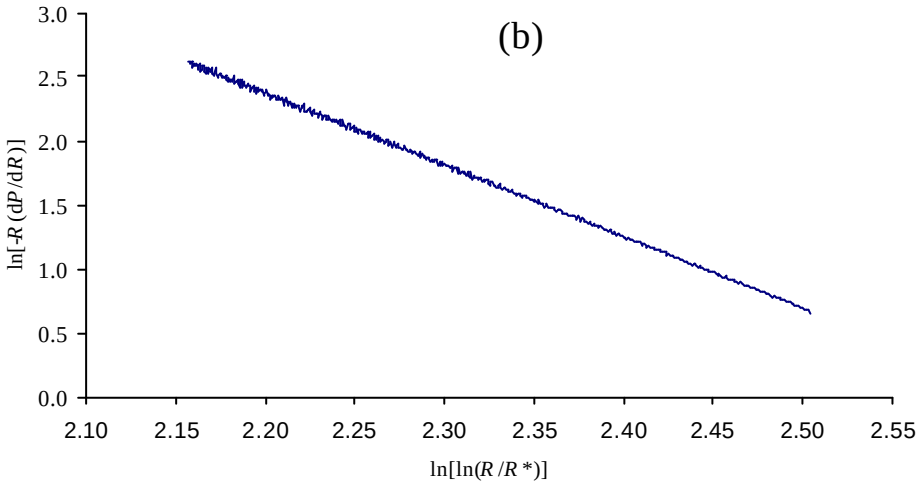

Figure 3: (a) χ^2 vs. R^* for fits to equation (17) for data from a synthetic load curve with 0.01% added noise generated using the standard parameter set at T_0 = 100 mK and Q = 0. The "best" value of R^* = 103.5 Ω. (b) The load curve data used in (b) plotted according to equation (17) using the "best" value of $R^* = 103.5\ \Omega$ as found above.

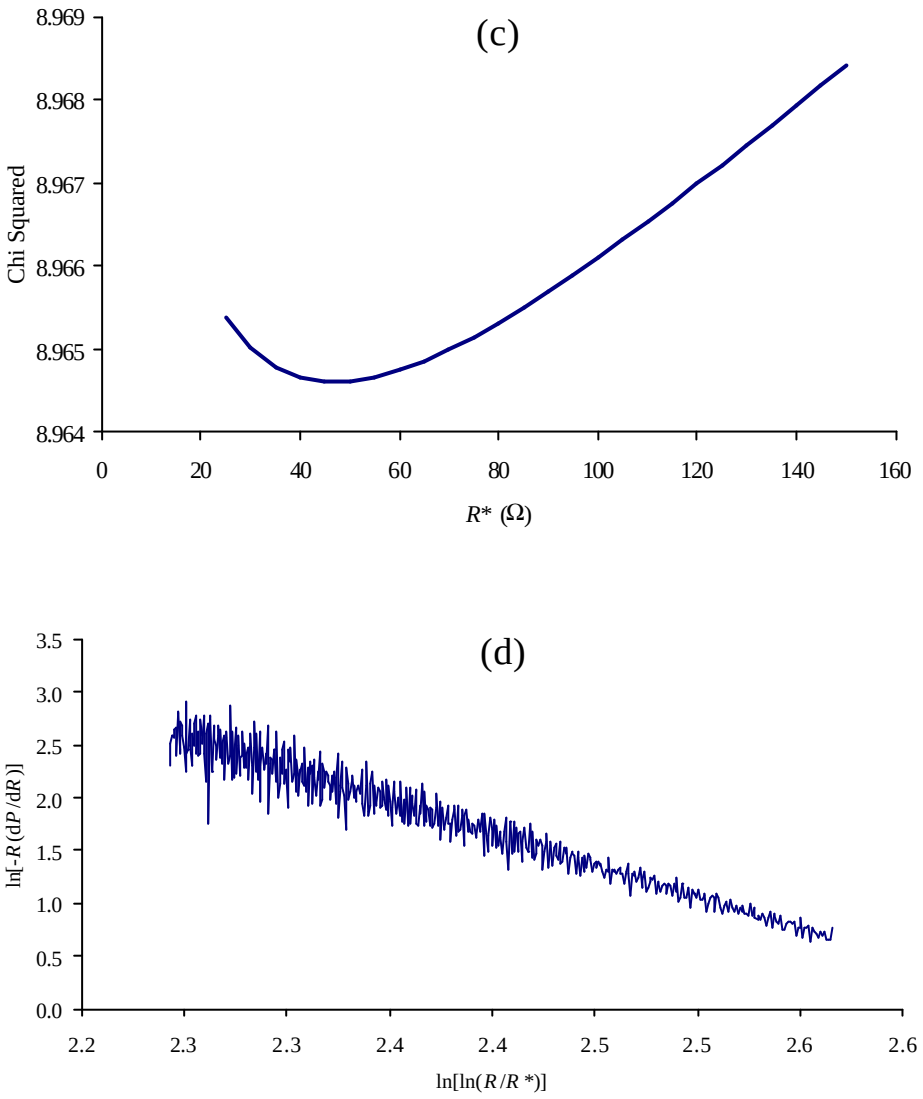

Figure 3: (c) χ^2 vs. R^* for fits to equation (17) for data from a synthetic load curve with 0.1% added noise generated using the standard parameter set at $T_0 = 100$ mK and $Q = 0$. The "best" value is $R^* = 47\ \Omega$; (d) the load curve data used in (c) plotted according to equation (17) using the "best" value of $R^* = 47\ \Omega$ as found above.

The other drawback with this approach is that from a single load curve it is not possible to say that the bolometer is truly running blanked. Thus, if there were any stray radiant

power absorbed during the measurement of a nominally blanked load curve, the derived values of T_g and hence G_{S0} would be erroneous.

In the following sections we show how these difficulties can be avoided by applying a non-linear fit to families of load curves recorded under different radiant loading conditions over a range of bath temperatures.

5 Non-linear fitting of load curves

Equations (6) and (8) can be combined into a form suitable for non-linear curve fitting:

$$\mathrm{P}(R) = X\left(\left(\frac{T_g}{T_0 \ln\left(\frac{R}{R^*}\right)^n}\right)^Y - 1\right) - Q, \tag{18}$$

where $Y = b + 1$ and $X = \frac{G_{S0} T_0}{Y}$. (19)

It is important to realise that one cannot simply fit X, Y, T_0, T_g, R^* and Q to measured data and expect a sensible result. (Remember that although T_0 is experimentally measured, in practise because of experimental and/or calibration errors we might wish to fit T_0 to the load curve data). The reason is that X, Y, T_0, T_g, R^* and Q are not independent parameters. For blanked load curves ($Q = 0$), T_0 is a function of T_g, R_0 and R^*:

$$T_0 = \frac{T_g}{\ln\left(\frac{R_0}{R^*}\right)^n}, \tag{20}$$

where R_0 is the thermistor resistance at zero bias current (and therefore zero electrical power). When Q is non-zero, it can be expressed as a function of X, T_g etc.:

$$Q = X\left(\left(\frac{T_g}{T_0 \ln\left(\frac{R_0}{R^*}\right)^n}\right)^Y - 1\right), \tag{21a}$$

$$T_0 < \frac{T_g}{\ln\left(\frac{R_0}{R^*}\right)^n}. \qquad (21b)$$

Furthermore, the parameter values for best fit are not unique. For example, if a set of parameters $\{b, T_g, R^*, G_{S0}, T_{01}\}$ fits a blanked load curve, the parameter set $\{b, T_g/f, R^*, fG_{S0}, T_{02}\}$ where $f = T_{01}/T_{02}$ will fit the load curve equally well. For non-blanked load curves the problem of degeneracy is compounded if we also attempt to fit Q as a free parameter. Mather [10] has already noted that the effect of dissipation of the absorbed radiant power in the bolometer is equivalent to that of operating the bolometer from a higher bath temperature but with less radiant power. More specifically, a non-blanked load curve defined by the parameters $\{b, T_g, R^*, G_{S0}, T_0, Q\}$ is identically reproduced by the parameter set $\{b, T_g, R^*, G_{S0}(f), fT_0, Q(f)\}$ where

$$G_{S0}(f) = G_{S0} f^b, \qquad (22a)$$

and

$$Q(f) = \frac{G_{S0}T_0}{b+1}\left[1 - f^{b+1}\right] + Q. \qquad (22b)$$

We note that for some range of f, $Q(f)$ is in fact negative which, although completely non-physical, actually reproduces the original load curve exactly. We note further that equation (22a) is completely consistent with a change in bath temperature and that $G_{d0} = G_{S0}$ at the new bath temperature.

We will return to this issue of degeneracy when discussing thermometry and non-blanked load curves but it is already clear that some parameters need to be determined prior to attempting a least squares fit. Fortunately, the family of blanked load curves affords the prior determination of both T_g and R^*.

6 Parameter derivation by fitting of load curve families

This section demonstrates a procedure for deducing the bolometer parameter set using load curve families recorded over a range of bath temperatures. We illustrate the procedure using noise free synthetic load curves generated using our standard parameter set. Practical issues are discussed in Section 7 using synthetic load curves with simulated noise added. In order to be representative of real experimental data, each synthetic load curve consists of a set of thirty current-voltage data points. Furthermore, the data points are more densely spaced at low bias currents, as is necessary [7] in order that a) the important quantity, R_0, can be more accurately measured and b) there be a sufficient number of data points in the linear portion of the load curve.

6.1 Blanked load curves

The importance of acquiring a good set of blanked load curves over a range of bath temperatures cannot be overstated as the data from this family provide the best

estimates of R^* and T_g through plotting $\ln[R_0(T_0)]$ vs. $1/T_0^n$. For bolometers using NTD-Ge thermistors, this curve is expected to be linear, of slope T_g^n and intercept $\ln(R^*)$. Departures from linearity will occur if the bolometer absorbs stray power, either due to a radiation leak or due to microphonic, electrical, or RF pickup. This provides a good test for the experimental setup. Figure 4 shows the curves determined from noise-free synthetic blanked load curves, and for synthetic load curves where a small stray power component, Q_s (= 0.05 pW, 0.1 pW and 0.2 pW), has been introduced. It is seen that the method not only determines R^* and T_g to very high accuracy for the case of the blanked load curves, but that for typical 100-mK bolometers, it is sensitive to stray power down to about 0.05 pW. We note that to detect departures from linearity in practice, we should extrapolate the linear fit to data points for high T_0, where the effect of stray power is minimal, to the lower values of T_0.

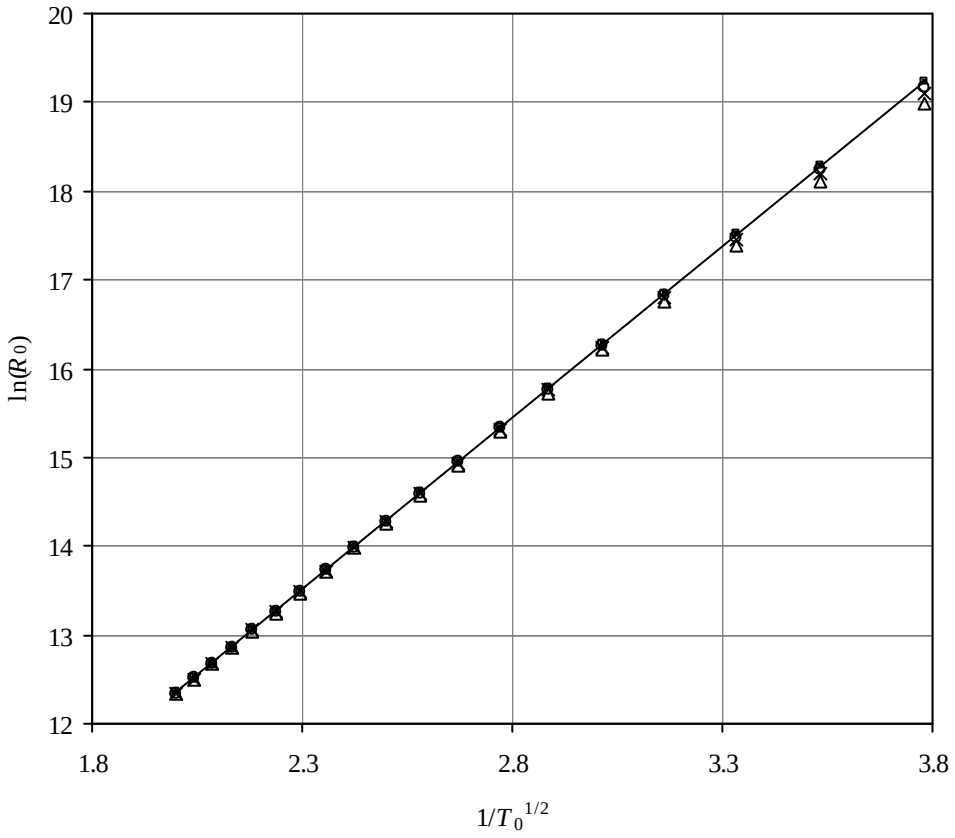

Figure 4: $\ln(R_0)$ vs. $1/T_0^{1/2}$ curves determined from noise-free synthetic load curves: blanked (solid squares and the fitted line); stray radiant power Q_s = 0.05 pW (open diamonds), 0.1 pW (crosses) and 0.2 pW (open triangles).

Having found R^* and T_g, and using equation (20), it is easy to demonstrate that a non-linear fit of the blanked load curves to equation (18) converges to determine X and Y (and hence G_{S0} and b) to high accuracy from a wide range initial guesses for X and Y. A synthetic non-blanked load curve and fit for T_0 = 100 mK is shown in upper trace of Figure 5.

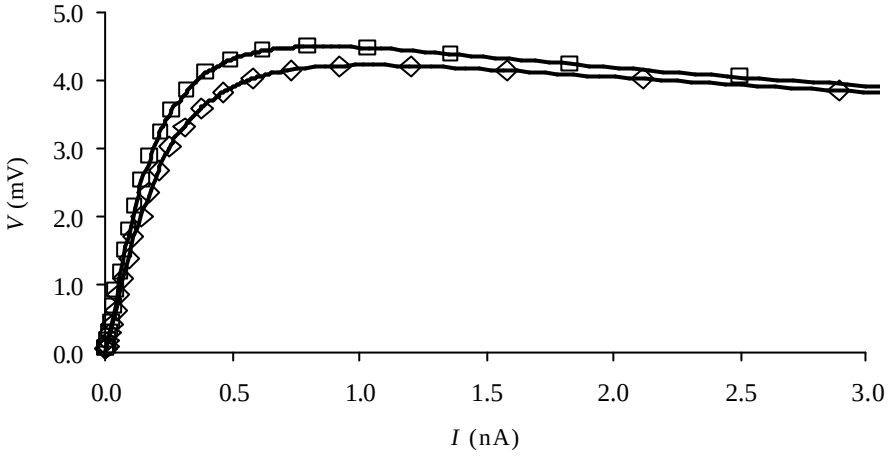

Figure 5: Synthetic noise-free load curves at T_0 = 100 mK: blanked (squares) and Q = 0.5 pW (diamonds). The lines are the model fits to the data.

6.2 Non-blanked load curves

Families of non-blanked load curves ($Q > 0$) are important because not only do they allow a measurement of the efficiency of the optical chain, but also because these data provide a means of checking the consistency of bolometer parameters. For these measurements, the beam of the bolometer optic is filled with radiation from a black body source at temperature T_{rad}. This is normally filtered to allow only radiation in the desired passband through, and reduced in intensity using neutral density filters to a level comparable to that expected in actual use. This results in a controlled amount of radiant power $Q(T_{rad})$ being absorbed by the bolometer. Again, families of load curves are measured over a range of bath temperatures. T_{rad} is typically 300 K for a black body source at room temperature or 77 K for a black body source at liquid nitrogen temperature. Woodcraft et al. [7] describe such measurements in detail.

The fitting procedure has been tested with synthetic noise-free non-blanked load curves calculated using the standard parameter set and Q = 0.5 pW. We assume that R^* and T_g have been determined from the family of blanked load curves (they cannot be determined from the non-blanked family). For the non-blanked load curves we combine equations (18) and (21a) to write $P(R)$ as

$$P(R) = X\left(\left(\frac{T_g}{T_0 \ln\left(\frac{R}{R^*}\right)^n}\right)^Y - 1\right) - X\left(\left(\frac{T_g}{T_0 \ln\left(\frac{R_0}{R^*}\right)^n}\right)^Y - 1\right). \quad (23)$$

X and Y can be readily fitted to equation (23). Again, the fits converge from a wide range of starting values for X and Y. The lower trace in Figure 5 shows a synthetic load curve together with the fit for $T_0 = 100$ mK.

Tests for internal consistency of the model are then:

(i) the calculated value of Q should be the same for all non-blanked load curves within a family recorded using a particular source temperature T_{rad};

(ii) the deduced values of b and G_{S0} should be the same for the blanked and non-blanked load curves recorded at the same bath temperature;

(iii) a curve of $\ln[G_{S0}(T_0)]$ vs. $\ln[T_0]$ should yield a straight line of slope b.

With synthetic noise-free data, the parameter recovery is, as expected, excellent. The following section describes how well this method works for synthetic load curves with noise added.

7 The influence of measurement errors on derived parameters

When attempting to fit real load curves, two important aspects must be considered: errors in the bath thermometer calibration and noise associated with measuring the load curves themselves.

7.1 Errors in the bath temperature, T_0

In order to plot $\ln[R_0(T_0)]$ vs. $1/T_0^{1/2}$, curves from a family of blanked load curves we clearly need a measure of the bath temperature T_0. In practice, a calibrated thermometer on the bolometer cold stage provides this. Errors in the calibration of this thermometer as well as errors in the measurement of R_0 will result in corresponding errors in the values of R^* and T_g. Before looking at how these errors affect the fitted values of G_{S0} and b within families of load curves, we discuss a more subtle point: namely, what value of T_0 should we use in the fits?

The obvious answer would be to use T_0 as measured by the calibrated thermometer. We assert here that the best approach for a consistent analysis of families of load curves is, in fact, to use the bath thermometer to determine the best estimates for R^* and T_g from the blanked load curves as described above; and then, having found R^* and T_g, to use T_0 as determined by equation (20). By doing this, random errors in both the calibration of

the stage thermometer and the measurements of R_0 are averaged over the data set. We are then effectively using the thermistor chip on the bolometer itself, for which equation (8) is known to be very good, as a sensitive heat bath thermometer.

7.2 The effects of errors in T_g and R^* on b and G_{S0}

It is easy to see the effect of an error in T_g on the best fit values of b and G_{S0}. If our deduced value of R^* is accurate, then any error in the value of T_g amounts to a systematic multiplicative error in thermistor temperature. That is, if we deduce a value T_g^{true}/f then equation (20) gives a bath temperature T_0/f. Likewise, the calculated thermistor temperature for any point on the load curve will be T/f instead of T. The net effect of this is that the non-linear fit then yields the values b and fG_{S0} with as good a fit as would have resulted had we been absolutely accurate in determining T_g. We note that equation (12) would also hold for these parameter values.

We demonstrate the effect of an error in R^* using the set of synthetic noise free blanked load curves generated using the standard parameter set. We use the exact value of T_g = 15 K but a range of values for R^* (80, 90, 100, 110, and 120 Ω). Table II lists the values of T_0 calculated using equation (20) and the fitted values of b and G_{S0} for synthetic load curves generated for bath temperatures of 100 mK, 170 mK and 250 mK. The important points to note are that if we underestimate R^*, the method returns a lower value for T_0 and higher values for G_{S0} and b, with b values increasing steadily with increasing base temperature. However, because the bolometer temperature depends only logarithmically on R^* we find that even for the load curve calculated with a base temperature of 250 mK, where the fits are worst, an error of 20% in R^* only amounts to an error of 5.5% in T_0. The corresponding errors in both G_{S0} and b are both 8.4%.

	100 mK			**170 mK**			**250 mK**		
R_* Ω	**T_0 mK**	b	**G_{S0} pW K^{-1}**	**T_0 mK**	b	**G_{S0} pW K^{-1}**	**T_0 mK**	b	**G_{S0} pW K^{-1}**
80	96.5	1.37	126.3	162.2	1.39	255.6	236.2	1.41	427.8
90	98.3	1.33	123.0	166.3	1.34	246.9	243.4	1.35	410.3
100	100	1.30	120.0	170.0	1.30	239.3	250.0	1.30	395.1
110	101.6	1.27	117.4	173.5	1.26	232.6	256.3	1.25	381.6
120	103.1	1.24	115.1	176.8	1.23	226.5	262.2	1.21	369.6

Table II: Calculated values of T_0 values from equation (20), and fitted b and G_{S0} values tabulated for a range of assumed R^* values for synthetic noise-free blanked load curves generated at base temperatures of 100 mK, 170 mK and 250 mK using the standard parameter set. T_g is taken as 15 K in the fits and calculations.

It is interesting to note that even though the fitted load curves generated using the parameters listed in Table II with T_g = 15 K are such that each they overlay the synthetic data well enough to be more or less indistinguishable, as the error in R^* increases so does the value of χ^2 for the fit. This suggests a strategy to improve our knowledge of R^*: plot χ^2 vs. R^* and use that value of R^* for which χ^2 is a minimum. Ideally, all load curves would return the same optimum value for R^*. However, it is easily demonstrated

that although a minimum in χ^2 is found for synthetic noise free load curves, in general no such minimum is found when noise is introduced even at only the 1% level.

7.3 Noisy synthetic load curves

We have seen that the methods described above work extremely well for synthetic noise free load curves. We now use families of synthetic blanked and non-blanked load curves with noise added at the 1% and 10% levels to test the applicability of the method to real data. Synthetic load curves were generated using the standard parameter set for range of bath temperatures $T_{0\mathrm{gen}}$ = {70 mK, 80 mK, … 250 mK.} For comparison, Figure 6 shows a 100-mK synthetic blanked load curve with 10% noise together with an experimentally measured blanked load curve for a prototype Planck HFI bolometer at T_0 = 98.5 mK (the solid lines are the fitted load curves, see below). It is clear that, systematic errors notwithstanding, a 10% noise level would represent poor data.

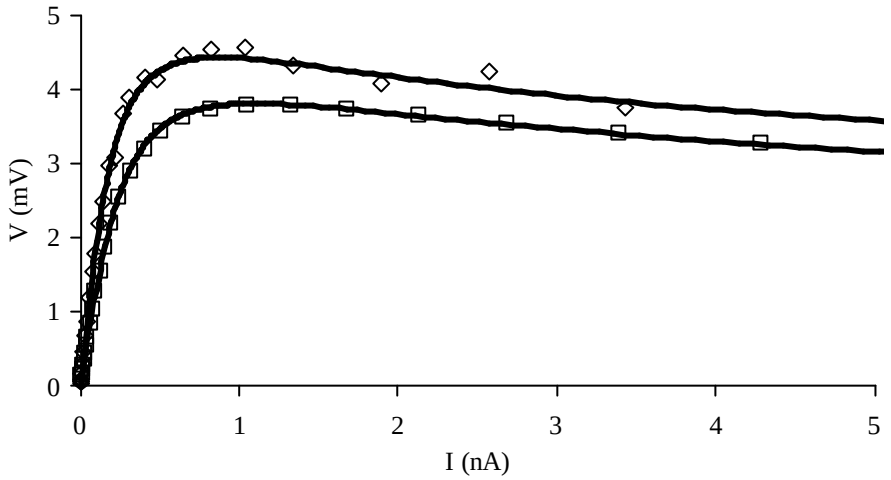

Figure 6: A synthetic blanked load curve with 10% noise generated using the standard parameter set at T_0 = 100 mK (diamonds) compared to a measured blanked load curve for a prototype Planck HFI bolometer, at T_0 = 98.5 mK (squares). The lines are fits to the data.

7.3.1 T_g and R^*

Figure 7 shows $\ln[R_0]$ vs. $1/T_{0\mathrm{noise}}^{1/2}$ curves for the synthetic 1% and 10% noise level blanked load curve data. The bath temperature used in this plot is $T_{0\mathrm{noise}} = T_{0\mathrm{gen}} + \Delta T_0$, where $T_{0\mathrm{gen}}$ is the temperature at which the load curve is generated and ΔT_0 is a random temperature fluctuation in the range ±1 mK. This would correspond to using the bath temperature as measured by the calibrated stage thermometer with a calibration error/noise level of ±1 mK. R_0 is estimated by averaging the resistance values of the first five data points from the load curve, over which the electrical power dissipation in the thermistor is sufficiently small that its resistance should remain essentially constant. We find that a linear fit yields values of $\{T_g = 15 \pm 0.005$ K, $R^* = 100 \pm 0.2\ \Omega\}$ for 1%

noise and $\{T_g = 15.1 \pm 0.09$ K, $R^* = 96.3 \pm 3\ \Omega\}$ for 10% noise. Thus, T_g and R^* are recovered to good accuracy (approximately 1% and 4%) even for noise levels of 10% on the load curves.

7.3.2 G_{S0} and b from blanked load curves

For blanked load curves, assuming that we have a measure of T_g and R^*, and setting $Q = 0$, the parameters $\{T_0, G_{S0}, b\}$ are independent. For the noise free synthetic blanked load curves we were able to calculate T_0 from R_0 using equation (20) confident that the value will be accurate. For noisy load curves, we have two options: either use R_0 in equation

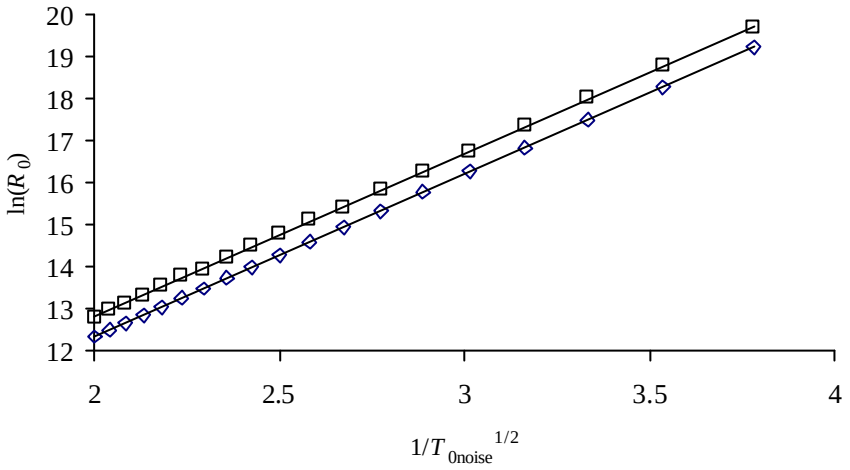

Figure 7: $\ln(R_0)$ vs. $1/T_{0noise}^{1/2}$ curves for synthetic blanked load curves with 1% added noise (diamonds) and 10% (squares). The 10% noise curve has been offset 0.5 units in the vertical direction for clarity. The lines are linear fits to the data.

(20) to calculate a value of T_0 to use in fits with $\{G_{S0}, b\}$ as free parameters, or fit $\{T_0, G_{S0}, b\}$ directly. We use the first of the two methods for the following reason: the best estimates for $\{T_g, R^*\}$ have been deduced using R_0 and T_{0noise}. Thus, the value T_0 given by equation (20) is the value most consistent with these T_g and R^* estimates. Fitting T_0 would return a value inconsistent with these $\{T_g, R^*\}$ values. It might be argued that having found a set of fitted T_0 values, these be used in the $\ln[R_0(T_0)]$ vs. $1/T_0^{1/2}$ plots to re-estimate $\{T_g, R^*\}$ and the process iterated. However, it is not clear that the process converges. In practice, fitting of synthetic non-blanked load curves suggest that the T_0 values found by the two methods are close enough to give identical $\{G_{S0}, b\}$ values to approximately 1% even for load curves with 10% noise.

Table 2 lists the calculated bath temperatures, T_0, and the fitted b and G_{S0} values for both the 1% and 10% noise level families of blanked load curves. Also listed in Table 2 for the 10% noise level family of load curves are the values if T_0 is fitted together with

G_{S0} and b rather than calculated from equation (20). The values demonstrate that the two methods yield more or less the same results. Figure 8 shows $\ln(G_{S0})$ vs. $\ln[T_0/T_0(100\text{ mK})]$ curves, where $T_0(100\text{ mK})$ is the calculated bath temperature for the 100 mK load curves. A linear fit to these curves yields $b = 1.304 \pm 0.005$ and $G_{S0}(100\text{ mK}) = 120.2 \pm 0.25$ pW K^{-1} for the 1% noise data, and $b = 1.26 \pm 0.06$ and $G_{S0}(100\text{ mK}) = 121.5 \pm 12$ pW K^{-1} for the 10% noise data. These "global" values for G_{S0} and b are in good agreement with those used to generate the load curves.

	1% Noise[a]			10% Noise[a]			10% Noise[b]		
T_{0gen} mK	T_0 mK	b	G_{S0} pW K^{-1}	T_0 mK	b	G_{S0} pW K^{-1}	T_0 mK	b	G_{S0} pW K^{-1}
70	70	1.31	74.9	70.2	1.27	78.7	70.4	1.27	79.7
100	100	1.29	120.4	99.9	1.44	115.2	99.9	1.45	113.3
150	150	1.31	202.8	148.5	1.14	216.0	150.4	1.10	228.4
200	200	1.30	296.0	198.8	1.44	289.0	199.3	1.43	291.7
250	250	1.28	397.7	251.2	1.70	326.5	240.5	1.86	225.1

[a] b and G_{S0} fitted with T_0 calculated using equation (20b)
[b] T_0, b and G_{S0} fitted

Table 2. Calculated[a] and fitted[b] values of T_0, and fitted values of G_{S0} and b tabulated for two families of synthetic noisy blanked load curves generated using the standard parameter set at bath temperatures of T_{0gen}.

7.3.3 G_{S0}, b and Q from non-blanked load curves

When faced with the task of fitting load curves with $Q > 0$, it is tempting to fit the data with T_0, G_{S0}, b, and Q as free parameters - see, for example, Naylor et al. [22]. We have shown in Section 6, however, that T_0, G_{S0}, and Q are not independent. With the synthetic noise-free non-blanked load curves of Section 6.2 we implicitly assumed prefect calibration of the bath thermometer and thus knew T_0, from which Q could be determined from equation (21a). Thus, we needed to only fit G_{S0} and b to the load curves.

With real data, if we ensure that the family of non-blanked load curves is recorded at the same set of bath temperatures as the family of blanked load curves (see Woodcraft et al. [7] for experimental details), then we can use those values of T_0 as determined by R^*, T_g and R_0 for the blanked load curves. Having fixed T_0 thus, we can either fit the data to $\{X, Y, Q\}$ (and hence $\{G_{S0}, b, Q\}$) in equation (18), or we can determine Q *a priori* and fit the data to $\{G_{S0}, b\}$. We can determine Q *a priori* in the same fashion as with the noise-free load curves: i.e., use R_0 in equation (21a) and fit $\{X, Y\}$ to equation (23).

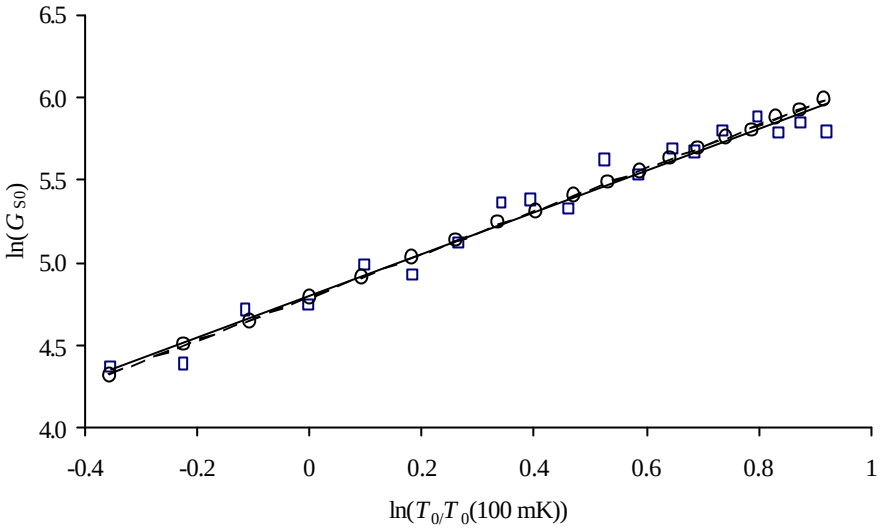

Figure 8: ln(G_{S0}) vs., Ln[T_0/T_0(100 mK)] curves from fitted {b, G_{S0}} parameters for blanked synthetic load curves. Circles and dashed line: 1% noise; squares and solid line: 10% noise.

Ideally both methods would return the same Q and the {G_{S0}, b} values would be consistent with those found for the family of blanked load curves.

These methods are demonstrated using families of synthetic non-blanked load curves, generated using the standard parameter set and Q = 0.5 pW, with 1% and 10% level added noise. Figure 9 shows the value of Q returned. It is seen that for both 1% and 10% level noise, using R_0 and fitting {X,Y} is marginally more accurate than fitting Q directly. With both methods, the value of Q is closer to the expected 0.5 pW for load curves generated at lower bath temperatures, which are more susceptible to the effect of radiant power loading. It is seen that for parameter set, the values of Q returned from the 10% noisy load curves become unreliable at bath temperatures much above 150 mK. Figure 10 shows that even with the large errors in Q at the higher bath temperatures, the {G_{S0}, b} values returned by the fits from both methods are in good agreement with expectations. These are summarised as {b, G_{S0}} = {1.31 ± 0.006, 119.5 ± 0.4 pW K^{-1}} and {1.34 ± 0.07, 122.3 ± 4.5 pW K^{-1}} obtained by fitting Q as a free parameter for the 1% and 10% noise level load curves, respectively, and {1.31 ± 0.005, 119.6 ± 0.3 pW K^{-1}} and {1.34 ± 0.06, 122.0 ± 3.8 pW K^{-1}} obtained by fitting {X, Y} to equation (23).

A second way to determine Q is to note that if two load curves are measured at the same base temperature and are looking at black body radiation from sources at temperatures T_{rad1} and T_{rad2}, then:

$$Q(T_{rad2}) - Q(T_{rad1}) = P(R,T_{rad2}) - P(R,T_{rad1}). \quad (24)$$

In particular, if the first load curve is measured with the bolometer blanked, then

$$Q = Q(T_{rad2}) = P(R,T_{rad2}) - P(R,blank). \quad (25)$$

Ideally, equation (25) would return the same value of Q for all values of R accessed by both $P(R)$ curves. With real noisy data, we would use the average value $\overline{Q}$ over the range R. This can be conveniently found by fitting both the blanked and non-blanked P-R data to a series expansion of the form

$$P(R) \approx F(R) = \sum_{j=-m}^{m} A_j R^j , \quad (26)$$

and calculating

$$\overline{Q} = \frac{\int_{R_{min}}^{R_{max}} [F(R,\text{blank}) - F(R,T_{\text{rad2}})]\,dR}{R_{\max} - R_{\min}}, \quad (27)$$

where ($R_{\max}$, $R_{\min}$) is the range of R common to both load curves. Equation (26) fits the load curves very well with m = 4 over the bath temperature range 70 - 250 mK considered here. Having calculated $\overline{Q}$, it can be used directly in equation (18) to fit {X, Y} as the only free parameters. The advantage of this method is that it uses the entire load curve to estimate Q. However, as Figure 11 shows, the values of $\overline{Q}$ found in this way are not as precise as for the other two methods described above. This is not surprising since effectively the errors in two load curves contribute the error in $\overline{Q}$.

8 Responsivity and *NEP*

The DC responsivity is defined by equations (13) and (14). It can be estimated from the low frequency limit of the speed of response measurements (see Ref. 7 for experimental details). Because it is difficult to have precise knowledge of the modulated power, what we actually obtain from these measurements is the normalised responsivity.

A second way of estimating the responsivity is by measuring two non-blanked load curves, one with the bolometer viewing a black body source at room temperature (300 K), the other viewing a black body source at liquid nitrogen temperature (77 K). We can use equation (24) and generalise equation (26) to measure the difference ΔQ between the two load curves. From the two load curves, we can measure the resultant change in voltage $\Delta V(I)$ and thus estimate the responsivity:

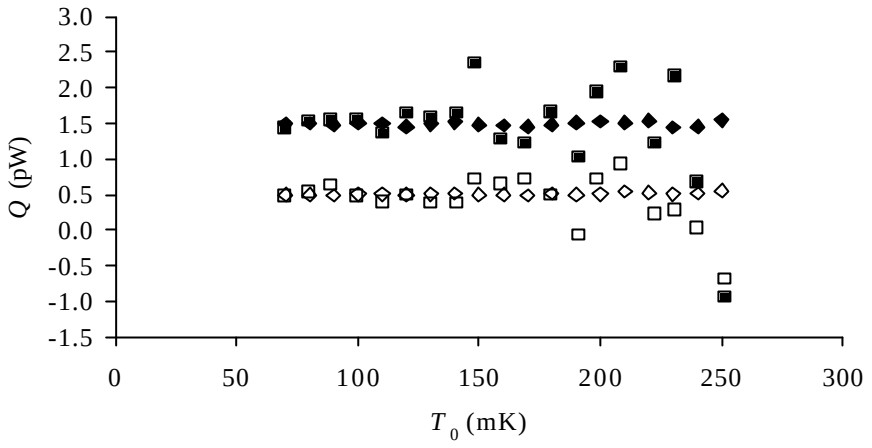

Figure 9: Q vs. T_0 for non-blanked noisy synthetic load curves. Open diamonds and open squares: using equation (23) for 1% and 10% noise load curves, respectively. Solid diamonds and solid squares: fitting Q as a free parameter for 1% and 10% noise load curves respectively (these are offset one by unit in the vertical axis for clarity.)

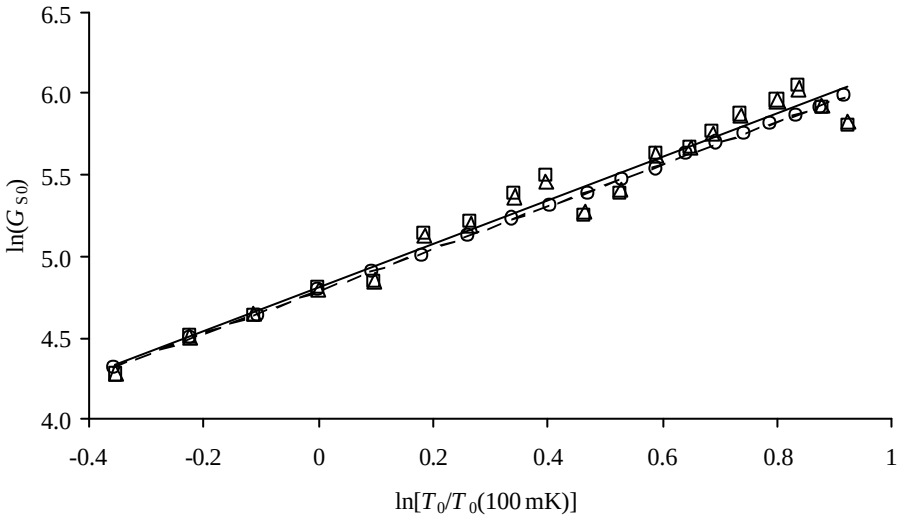

Figure 10: $\ln(G_{S0})$ vs., $\ln(T_0/T_0(100\text{ mK}))$ curves from fitted $\{b, G_{S0}\}$ parameters for synthetic non-blanked load curves. Circles and dashed line: 1% noise and fits using equation (23); triangles and solid line: 10% noise and fits using equation (23); squares: 10% noise and fitting Q as a free parameter.

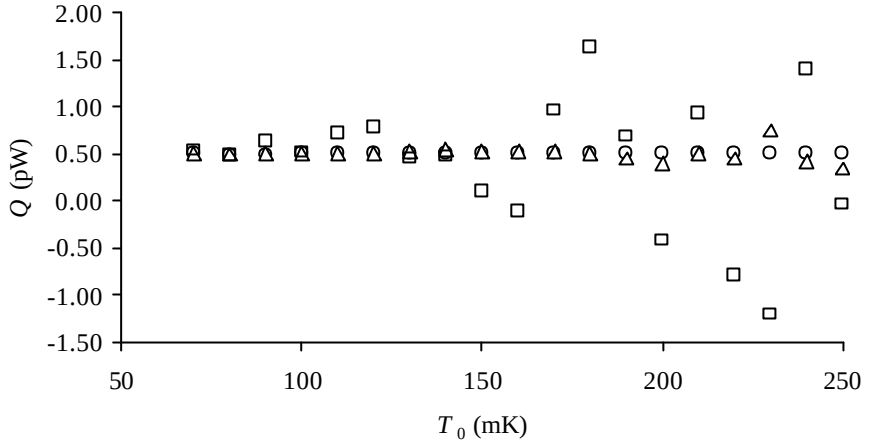

Figure 11: Q vs. T_0 for non-blanked noisy synthetic load curves using equation (26). circles: zero noise; triangles: 1% noise; squares: 10% noise.

$$S \approx \frac{\Delta V(I)}{\Delta Q}. \qquad (28)$$

We stress that equation (27) will always underestimate the responsivity to some degree: by definition responsivity is the small signal response whereas neither ΔV nor ΔQ (even with heavy filtering) are necessarily small in this method.

Our measurements on real bolometers [5, 7] show that not only does the ideal thermal model fit the load curves very well, but that both the normalised responsivity and the absolute responsivity estimated by equation (27) are also well reproduced. This demonstrates the validity of our experimental technique, but should it increase our confidence in the parameter set found by these methods? The answer is, unfortunately, no. It is clear from equations (13) and (14) that the responsivity depends only on the shape of the load curve. Thus, any parameter set that describes the load curve accurately will give the same responsivity. This can be seen in Figure 12, which shows responsivity curves, $S(I)$, for three parameter sets $\{T_0, R^*, T_g, b, G_{S0}, Q\}$ = {100 mK, 100 Ω, 15 K, 1.3, 120 pW K^{-1}, 0.5 pW}, {70 mK, 100 Ω, 15 K, 1.3, 75.5 pW K^{-1}, 3.42 pW} and {100 mK, 50 Ω, 20 K, 1.515, 80 pW K^{-1}, 2.28 pW}, all of which describe the same load curve with good accuracy. The three responsivity curves corresponding to the three parameter sets overlay extremely accurately. Similarly, the forms of equations (A10), (A11) and (A12) for the total intrinsic *NEP* suggest that any parameter set describes the load curve well, will also give the same $NEP(I)$ curve.

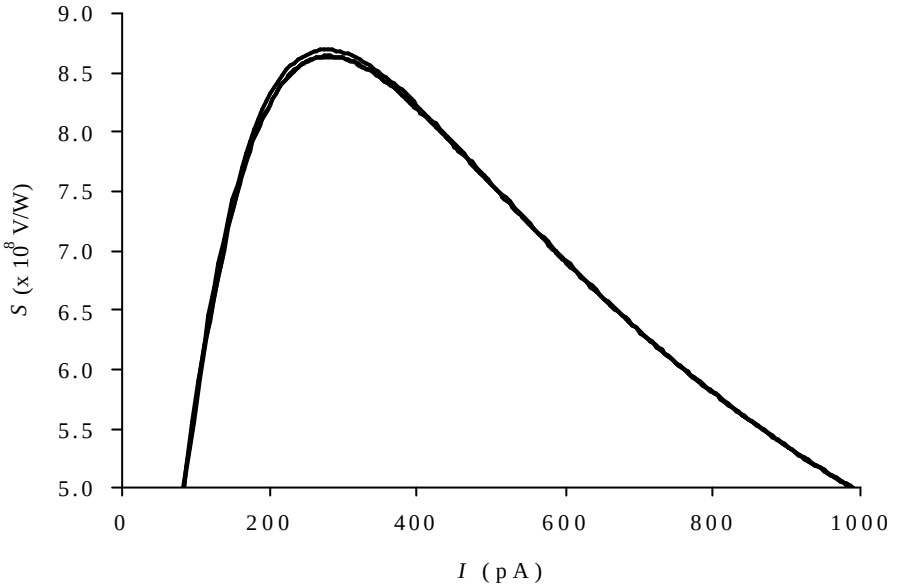

Figure 12: Calculated optical responsivity vs. bias current for the three parameter sets $\{T_0, R^*, T_g, b, G_{S0}, Q\}$ = {100 mK, 100 Ω, 15 K, 1.3, 120 pW K^{-1}, 0.5 pW}, {70 mK, 100 Ω, 15 K, 1.3, 75.5 pW K^{-1}, 3.42 pW} and {100 mK, 50 Ω, 20 K, 1.515, 80 pW K^{-1}, 2.28 pW}. The first two curves overlay exactly (lower curve), the third (upper curve) almost so.

9 Departures from the ideal thermal model

A critical examination of experimental results and model fits presented by Sudiwala et al. [5] and Woodcraft et al. [7] suggests a departure from ideal thermal behaviour NTD-Ge bolometers at bath temperatures below about 100 mK. This cannot be accounted for consistently by invoking only the electric field effect described by equation (7). It is possible that the departures are due to a combination of factors, such as the electric field effect, electron-phonon decoupling [20], or thermal drift of the heat bath and amplifier gain errors, all which become more acute at lower bath temperatures. These issues will be addressed in future modelling and experiments.

10 Conclusions

We have revised and extended the Griffin & Holland ideal thermal model for NTD bolometer behaviour and presented a method by which bolometer parameters can be extracted from experimental data. Problems of bolometer characterisation resulting from parameter degeneracy have been discussed. We have demonstrated how these problems can be overcome through measuring families of load curves over a range of bath

temperatures. The importance of a family of blanked load curves for the determination of R^* and T_g cannot be over-stressed. We have shown that from this family of blanked load curves G_{S0} and b can obtained through non-linear fitting of *R-P* curves. Using this knowledge of R^* and T_g families of non-blanked load curves then serve as a check for consistency by comparing the values of G_{S0} and b obtained from fitting these load curves to those obtained previously. A further test of consistency is afforded by the values of absorbed radiant power derived from these fits. We have shown that whereas optical responsivities do not serve as a further test for consistency, that *NEP*s do. Finally, it has been shown that parameter recovery is possible to reasonable accuracy even from relatively noisy data sets.

The final assessment of the applicability of the ideal thermal model in describing real devices can only be validated by experimental measurements. The results presented by Woodcraft et al. [7] for two such devices, and earlier results by Sudiwala et al. [5], indicate that the model is able to describe real devices over useful temperature ranges.

Appendix

We reformulate the important equations of Griffin & Holland taking into account the power law variation of the thermal conductivity rather than the thermal conductance. We define

$$f = \frac{T}{T_0} \qquad d = \frac{T_g}{T_0} \qquad g = \frac{Q}{G_{S0}T_0}. \tag{A1}$$

Equations (6) and (10) can be written as:

$$P = G_{S0}T_0\left[\frac{\left(f^{b+1}-1\right)}{b+1} - g\right], \tag{A2}$$

and

$$a = -\frac{nd^n}{T_0 f^{n+1}}. \tag{A3}$$

For infinite load resistance equations (13) and (14) become:

$$S = \frac{Z-R}{2V} = \frac{aV}{G_e}, \tag{A4}$$

and

$$G_e = G_d - aP. \tag{A5}$$

A.1 DC responsivity

Combining equations (11), (13), (A1) and (A2) the DC responsivity can be expressed in terms of bolometer parameters as

$$|S| = \left(\frac{R^*}{G_{S0}T_0}\right)^{1/2} \left[\frac{nd^n\left\{exp\left[\left(\frac{d}{f}\right)^n\right]\left[\frac{\left(f^{b+1}-1\right)}{b+1}-g\right]\right\}^{1/2}}{f^{b+n+1}+nd^n\left[\left[\frac{\left(f^{b+1}-1\right)}{b+1}-g\right]\right]}\right]\left(\frac{R_L}{Z+R_L}\right). \quad \text{(A6)}$$

For infinite load resistance (i.e., constant current bias), this reduces to

$$|S| = \left(\frac{R^*}{G_{S0}T_0}\right)^{1/2} \left[\frac{nd^n\left\{exp\left[\left(\frac{d}{f}\right)^n\right]\left[\frac{\left(f^{b+1}-1\right)}{b+1}-g\right]\right\}^{1/2}}{f^{b+n+1}+nd^n\left[\left[\frac{\left(f^{b+1}-1\right)}{b+1}-g\right]\right]}\right]. \quad \text{(A7)}$$

Equation (A7) is the revised form of Griffin & Holland's equation (18).

A.2 Variation of responsivity with background power

Griffin & Holland investigated the variation of responsivity with background power normalised to the responsivity of the bolometer operating under some loading Q_a for the special case of Q_a=0. For the more general case of $Q_a > 0$, but still with infinite load resistance, we find

$$g = \left(\frac{1}{b+1}\right)\left[\left(f^{b+1}-1\right) - \left[\left(f_a^{b+1}-1\right) - g_a(b+1)\right]\exp\left[\frac{d^n\left(f_a^n - f^n\right)}{(ff_a)^n}\right]\right], \quad \text{(A8)}$$

$$\text{and} \quad \frac{S}{S_a} = \frac{f_a^{b+n+1} + nd^n\left(\frac{f_a^{b+1}-1}{b+1} - g_a\right)}{\exp\left[\frac{d^n\left(f^n - f_a^n\right)}{(ff_a)^n}\right] f^{b+n+1} + nd^n\left(\frac{f_a^{b+1}-1}{b+1} - g_a\right)}, \quad \text{(A9)}$$

where g_a and f_a define the initial operating point of the bolometer with responsivity S_a, and g and f define the new operating point with responsivity S. Setting $g_a = 0$ in

equations (A8) and (A10) yields the revised forms of Griffin & Holland's equations (25) and (26).

A.3 Noise Equivalent Power

The intrinsic *NEP* of an ideal thermal bolometer is given by

$$NEP^2 = NEP_J^2 + NEP_P^2, \tag{A10}$$

where NEP_J is the Johnson noise component and NEP_P is the phonon noise component. Following the non-equilibrium noise analysis of Mather [10], these components can be expressed as

$$\begin{aligned} NEP_J^2 &= \frac{kT(R+Z)^2}{RS^2}\left[1+w^2t^2\right]^{1/2} \\ &= 4kT_0^2G_{S0}\left[\frac{f^{2(b+n+1)+1}}{n^2d^{2n}\left(\frac{f^{b+1}-1}{b+1}-\right)}\right]\left[1+w^2t^2\right]^{1/2}, \end{aligned} \tag{A11}$$

where $t = C/G_d$ is the thermal time constant; and

$$NEP_P^2 = 4k(qT)^2 G_d, \tag{A12}$$

where $q < 1$ and accounts for the temperature gradient between the bolometer element and the thermal bath. If t and $g(t)$ are the temperatures and thermal conductances, respectively, along the length of the thermal link, then

$$(qT)^2 = \left(\frac{1}{g(T)}\right)\frac{\int_{T_0}^{T}[tg(t)]^2\,dt}{\int_{T_0}^{T} g(t)dt}. \tag{A13}$$

Integrating equation (A13) gives

$$q^2 = \left(\frac{1}{f^{b+2}}\right)\left(\frac{f^{2b+3}-1}{f^{b+1}-1}\right)\left(\frac{b+1}{2b+3}\right), \tag{A14}$$

from which, together with equation (A12), we can obtain

$$NEP_P^2 = 4kT_0G_{S0}\left(\frac{f^{2b+3}-1}{f^{b+1}-1}\right)\left(\frac{b+1}{2b+3}\right). \qquad \text{(A15)}$$

Equations (A11) (with $w = 0$) and (A15) are the revised forms of Griffin & Holland's equations (19) and (20).

References

[1] Holland, W S, E I Robson, W K Gear, C R Cunningham, J F Lightfoot, T, Jenness, R J Ivison, J A Stevens, P A R Ade, M J Griffin, W D Duncan, J A Murphy, and D A Naylor. *Mon. Not. R. Astron. Soc.* 303, 659, 1999.

[2] Piacentini, F, P A R Ade, R Bathia, J J Bock, A Boscaleri, P Cardoni, B P Crill, P de Bernardis, H Del Castillo, G de Troia, P Farese, M Giacometti, E F Hivon, V V Hristov, A Iacoangeli, A E Lange, S Masi, P D Mauskopf, L Miglio, C B Netterfield, P Palangio, Pascale, A Raccanelli, S Rao, G Romeo, J Ruhl, and F Scaramuzzi (submitted to *Ap. J.*)

[3] Griffin M J, B M Swinyard, and L Vigroux. *Proc. Symposium "The Promise of FIRST",12-15 Dec. 2000, Toledo, Spain ESA-SP 460* (in press).

[4] Mauskopf, P D, J J Bock, H Del Castillo, W L Holzapfel, and A.E. Lange. *Appl. Opt.* 36 765, 1997.

[5] Sudiwala, R V, B Maffei, M J Griffin, C V Haynes, P A R. Ade, R S Bhatia, A D Turner, J J Bock, A E Lange, and J W Beeman, *Nucl. Instr. and Meth. A* 444, 413, 2000.

[6] Turner, A D, J J Bock, J W Beeman, J Glenn, P C Hargrave, V V Hristov, H T Nguyen, F Rahman, S Sethuraman, and A L Woodcraft. *Appl. Opt.*, 40, 4291, 2001

[7] Woodcraft, A L, R V Sudiwala, M J Griffin, E Wakui, B Maffei, C E Tucker, C V Haynes, F Gannaway, P A R Ade, J J Bock, A D Turner, and S Sethuraman. *Int. J. Infrared. Mill. Waves*, 23, 575 (2002).

[8] Jones, R Clark, *J. Opt. Soc. Am.* 43, 1, 1953.

[9] Low, F J, *J. Opt. Soc. Am.* 51, 1300, 1961.

[10] Mather, J C, *Appl. Opt.* 21, 1125, 1982.

[11] Mather, J C, *Appl. Opt.* 23, 584, 1984.

[12] Chanin, G, & J P Torre, *J. Opt. Soc. Am. A*, 1, 412, 1984.

[13] Griffin, M J, & W S Holland, *Int. J. Infrared Mill. Waves*, 9, 861, 1988.

[14] Grannan, S M, P L Richards, and M K Hase, *Int. J. Infrared Mill. Waves*, 18, 319, 1997.

[15] Murray, A G, P A R Ade, J Beeman, R S Bhatia, J J Bock, H D Castillo, M J Griffin, A Lange, B Maffei, and R Nartallo. *Proc. 30th ESLAB Symposium, "Submillimetre and Far-infrared Space Instrumentation"*, 24-26th Sept. 1996, ESTEC, Noordwijk, The Netherlands, ESA SP-388, 1996

[16] Richards, P L, *J. Appl. Phys.* 76, 1, 1994.

[17] Hill, R M, *Philos. Mag.* 24, 1307, 1971.

[18] Grannan, S M, A E Lange, E E Haller, and J W Beeman, *Phys. Rev. B.* 45, 4516, 1992.
[19] Efros, A L, & B I Shklovski, *J. Phys. C*, 8, L49-51, 1975.
[20] Wang, N, F C Wellstood, B Sadoulet, E E Haller, and J Beeman, *J. Am. Phys. Soc.*, 41, 376, 1990.
[21] Pobell, F, *Matter and Methods at Low Temperatures*, Springer, 1992.
[22] Naylor, D A, B G Gom, P A R Ade, and J E Davis, *Rev. Sci. Instr.* 70, 4097, 1999.